Reduction of Cogging Torque and Torque Ripple in Interior PM Machines With Asymmetrical V-Type Rotor Design

Wu Ren, Qiang Xu, Qiong Li, and Libing Zhou

School of Electrical and Electronic Engineering, Huazhong University of Science and Technology, Wuhan 430074, China

High cogging torque is a common drawback of the interior permanent magnet machine. In this paper, a novel technique is adopted to reduce cogging torque and torque ripple by using an asymmetrical V-type rotor configuration. First, the analysis modes are presented, and the proposed rotor is optimized by the hybrid design of experiment. A satisfactory set of parameters is determined. Next, the cogging torque and the torque ripple of the proposed model are compared with those of the basic model. The results demonstrate that the cogging torque and the torque ripple are reduced significantly by the adoption of the proposed rotor. Then, the performance of the proposed model rotating clockwise is compared that of the proposed model rotating counterclockwise to evaluate the effectiveness of the proposed rotor. Finally, the validity of the proposed method is confirmed by experiment.

***Index Terms*— Asymmetrical V-shape rotor configuration, high cogging torque, hybrid design of experiments (DOEs), interior permanent magnet (IPM) machine.**

I. Introduction

THE interior permanent magnet (IPM) machines have been widely used in electrical vehicles, home applications, and industrial applications. The IPM machines exhibit high torque density and efficiency due to salient rotor structure. However, due to this rotor, IPM machines contain high cogging torque [1]. The cogging torque is a major source for the torque ripple of PM machine, which results in mechanical vibration and acoustic noise and affects drive system performance [2], [3]. A reduction of the cogging torque is highly crucial for a smooth electromagnetic torque. Many previous techniques have been reported for reducing the cogging torque, such as the skewing technique [1], pole-arc coefficient optimization [4], rotor with unequal outer diameter and stator with pole shoe modification [5], notches put on the rotor pole face [6], double-barrier rotor [7], rotor axial segment and twisting with respect to each other [8], asymmetric rib design and inverting inverting lamination [9], and magnet shifting [10]. In [11], an asymmetrical V-type rotor is proposed for effectively reducing the cogging torque. But this machine can demonstrate different torque ripples from different rotatory directions.

In order to deal with the drawback of the rotor presented in [11], a novel asymmetrical V-type rotor is proposed to reduce cogging torque and torque ripple in the bidirectional operation, without deteriorating other machine performance, as well as increasing rotor complexity and manufacturing cost. In order to accurately calculate torque characteristics, finite element modeling is built, and the commercial finite element analysis (FEA) software is used. The hybrid design of experiment (DOE) is adopted for rotor optimization, i.e., Taguchi method combining with parameter sweep method. Hybrid DOE contributes to improving efficiency and quality of design optimization. A significant reduction of the cogging torque and the torque ripple is achieved by the proposed rotor.

Manuscript received November 3, 2015; revised December 28, 2015; accepted February 13, 2016. Date of publication February 18, 2016; date of current version June 22, 2016. Corresponding author: Q. Xu (e-mail: powerdsp@hust.edu.cn).

Color versions of one or more of the figures in this paper are available online at http://ieeexplore.ieee.org.

Digital Object Identifier 10.1109/TMAG.2016.2530840

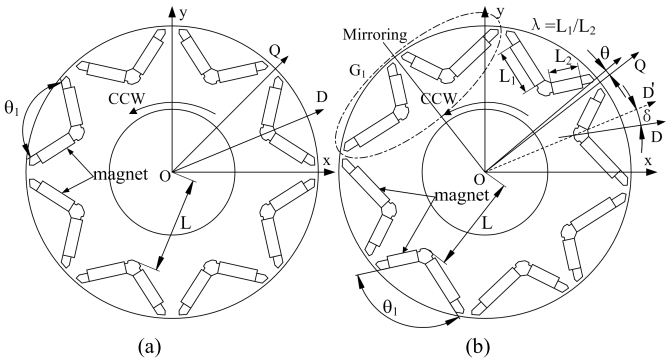

Fig. 1. V-type rotor comparison. (a) Conventional rotor. (b) Proposed rotor.

II. Analysis Model and Design Optimization

A. Analysis Model

Fig. 1 shows the rotor cross section of the conventional and novel V-type structure. In Fig. 1(a), the rotor is equipped with the symmetry V-type barriers, and two uniform magnets are symmetrically distributed on both sides of the pole-pitch centerline OD. In addition, eight V-type barriers are arranged by circular array. In Fig. 1(b), the novel rotor structure is evolved from that presented in [11]. Note that there are also three striking features for this rotor: 1) V-type barrier shifts at an angle of δ to the pole-pitch centerline; 2) width of magnets in the barrier is nonuniform; and 3) every two barriers constitute a group (G_1) by mirroring, and they are arranged by the adoption of circular array for four groups. Three important dimensions are selected as design variables for optimization, as shown in Fig. 1(b):

1) δ: shifting angle of V-type barrier to the pole-pitch centerline;
2) λ: ratio of magnet I width to magnet II width;
3) θ: rotation angle of V-type barrier against the q-axis.

The optimization model is obtained under the assumption that machine rotates counterclockwise (CCW). In Section IV, the CW performance of the optimized model is evaluated. All models have the same design conditions, as shown in Table I. In addition, stator has a single-layer winding of the short pitched coil by three or four slots.

TABLE I
MAIN SPECIFICATIONS OF IPM MACHINES

Parameters	Value	Unit
Outer diameter of stator, D_{os}	170	mm
Outer diameter of rotor, D_{or}	107	mm
Angle between two permanent magnet, θ_1	110	°
Thickness of permanent magnet, d_m	4.3	mm
Total width of permanent magnet, w_m	28	mm
Air gap length, g	1.0	mm
Stack length, L_a	66	mm
No. of slots	36	-
No. of poles	8	-
Residual flux density of PM	1.2	T

TABLE II
DESIGN AREA AND LEVEL OF DESIGN VARIABLES

Variable	Min	Max	Level
λ(-)	14/14	18/10	15.5/12.5,16.5/11.5,17.5/10.5
θ(°)	0	3	2.0,2.2,2.4
δ(°)	0	16	8,10,12

TABLE III
TORQUE CHARACTERISTICS OF NINE IPM MODELS USING FEA

Model	λ(-)	δ (°)	θ (°)	T_{cog}(N·m)	T_{avg}(N·m)	$\triangle T$ (%)
1	15.5/12.5	2.0	8	1.69	10.26	20.37
2	15.5/12.5	2.2	10	1.22	10.25	14.86
3	15.5/12.5	2.4	12	0.83	10.18	9.66
4	16.5/11.5	2.0	10	1.45	10.24	17.65
5	16.5/11.5	2.2	12	0.70	10.18	8.62
6	16.5/11.5	2.4	8	1.37	10.25	16.77
7	17.5/10.5	2.0	12	1.02	10.16	12.21
8	17.5/10.5	2.2	8	1.59	10.26	19.52
9	17.5/10.5	2.4	10	0.99	10.24	12.75

T_{cog}= cogging torque, $\triangle T$ =peak-to-peak value/ average torque.

B. Asymmetrical Rotor Optimization Using Hybrid DOE

The Taguchi method is used to redefine the design area of variable. Table II shows the design area and level of design variables, which are determined by considering manufacturing error and dimensional constraint. Nine motor models corresponding to a standard orthogonal array L_9 (3^3) are built for Taguchi method, as shown in Table III. Calculated results of cogging torque and torque ripple are also shown in Table III. Model 5 shows the least cogging torque. In addition, the torque ripple retains the similar reduction trend as cogging torque. Fig. 2 shows the main effect of each factor on cogging torque. Design areas of parameters for the minimization of the cogging torque are determined, $\lambda \in$ (16.5/11.5, 17.5/10.5), $\theta \in$ (2.4, 2.8), and $\delta \in$ (12, 15).

Analysis of variance is applied to determine the importance of design variable to design objective. Calculation results are shown in Table IV. Shifting angle δ and magnet width λ have an important effect on the cogging torque. More sweep points are set for fine calculation. Local optimization is carried out in the refined design area, and parameter sweep method is applied to search a satisfactory set of design parameters from sweep points. Further research has found that when λ and δ are determined, θ have a huge impact on the cogging torque. After many experiments, the final design parameters are determined, i.e., $\lambda = 17/11$, $\delta = 14°$, and $\theta = 1.97°$.

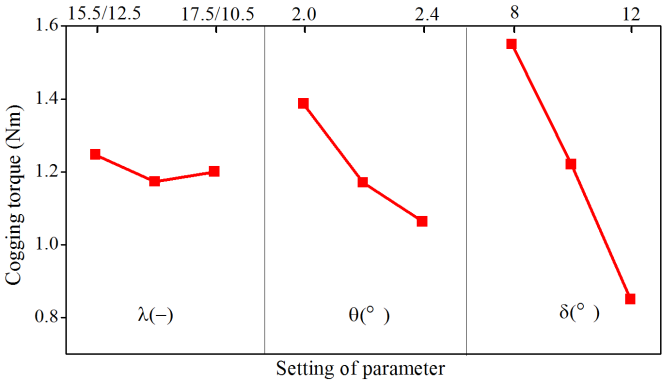

Fig. 2. Main factor effects on the cogging torque.

TABLE IV
EFFECTS OF ALL FACTORS ON MACHINE PERFORMANCE

Factors	T_{cog}(N·m)		$\triangle T$ (%)	
	SS	Factor effect (%)	SS	Factor effect (%)
λ(-)	0.0083	0.91	0.629	0.46
θ(°)	0.1629	17.96	20.996	15.39
δ(°)	0.7358	81.13	114.776	84.15
sum	0.9069	100	136.402	100

SS=sum of square

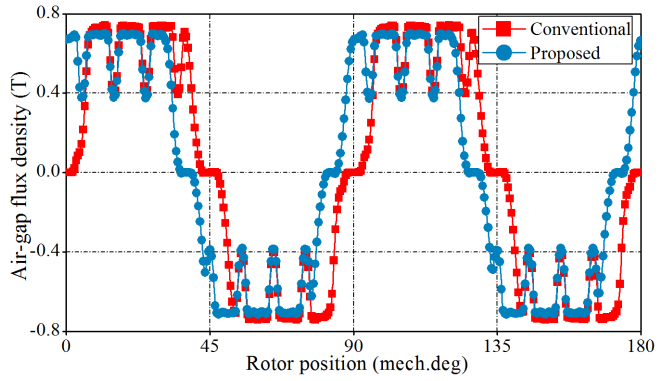

Fig. 3. Air-gap flux distribution for the two models.

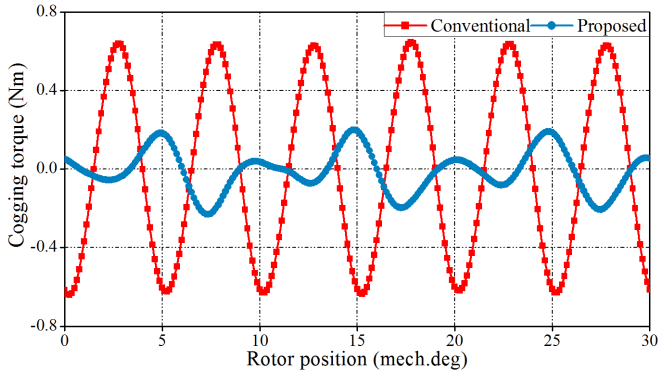

Fig. 4. Cogging torque comparison for the two models.

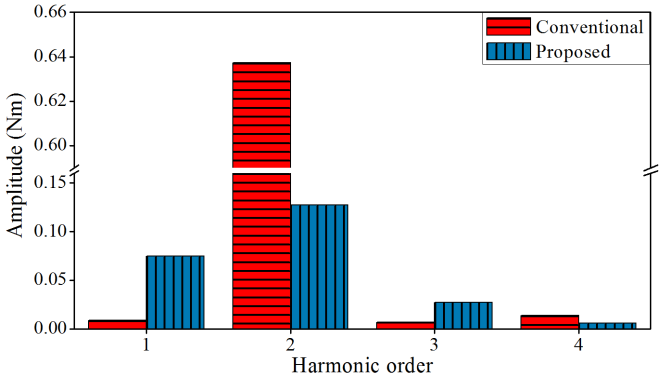

Fig. 5. Harmonics analysis of cogging torque.

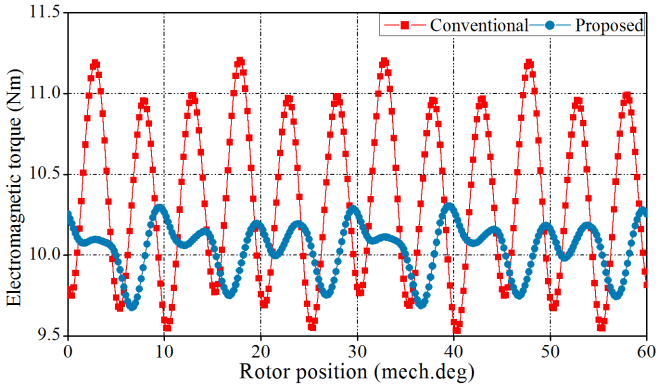

Fig. 6. Electromagnetic torque comparison for the two models.

III. Performance Comparison

A. Flux Density Distribution

Fig. 3 shows the open-circuit air-gap field distributions for two structures. Both of them are approximate to the rectangular waveforms due to the adoption of flat magnets. The proposed model shows slightly lower waveform amplitude, as compared with the conventional one. Moreover, there exists remarkable phase shifting between two waveforms.

B. Cogging Torque Comparison

Fig. 4 shows the comparison of cogging torque for the two models. Theoretically, the mechanical angle corresponding to each period of the cogging torque [$\theta_{\text{cog}} = 360°/\text{LCM}(36, 8) = 5°$, LCM is the least common multiple] is 5°. But the proposed model shows the period as 10° due to the adoption of this rotor. The proposed model contains the peak-to-peak value as 0.43 N · m, which is reduced by 66.67%, as compared with that of the conventional one as 1.29 N · m. It can be concluded that the proposed rotor gives main contribution for a reduction of cogging torque. In order to evaluate the effectiveness of the proposed rotor, a fast Fourier transform (FFT) analysis is used in this paper. The mechanical angle of 10° is used to carry out the FFT analysis. The dominant harmonics of cogging torque are the multiples of the second harmonic, and the FFT analysis results are shown in Fig. 5. The torque harmonic of the second order gives main contribution to a reduction of cogging torque. The amplitude of the second order of the proposed model is 0.128 N · m, which is reduced by 79.9%, as compared with that of the conventional model as 0.637 N · m.

C. Electromagnetic Torque Comparison

Two models are fed with a three-phase sinusoidal current excitation. Fig. 6 shows the electromagnetic torque for the two models when $I = 6$ A. Due to the different rotors, two models obtain the maximum average torque at various current phase angles β, i.e., 0.14 and −0.29 rad, respectively. The proposed model shows more smooth electromagnetic torque. The torque ripple of the proposed model is 6.26%, 9.96% less than that of the conventional one. But, it is worth noticing that they have approximate average torque, 10.36 and 10.04 N · m. The proposed rotor makes little difference to average torque.

Table V shows the performance comparisons of the two models.

TABLE V
Performance Comparisons for the Two Models

Items	Unit	Conventional model	Proposed model	
			CCW	CW
T_{cog}	N·m	1.29	0.43	0.44
β	rad	0.14	-0.29	0.6
T_{avg}	N·m	10.36	10.04	10.12
$\triangle T$	%	16.22	6.26	6.67

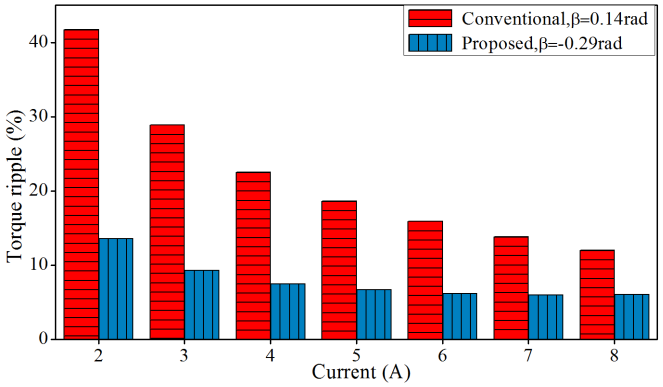

Fig. 7. Torque ripple versus current, at a constant current phase angle.

D. Torque Ripple at Various Currents

In an application of plastic injection molding, the maximum torque per ampere control is adopted in the machines, without field weakening control. Hence, current phase angle β is set as a constant, and the electromagnetic torque is calculated by FE at various currents. Fig. 7 compares the torque ripple versus current. The proposed model shows lower torque ripple than the conventional one at each current. When $I = 2$ A, the ripple value of the proposed model is 13.58%, 28.16% less than that of the conventional one. When $I = 8$ A, the ripple value of the proposed model is 6.03%, 5.98% less than that of the conventional one. This design technique also proves to be very effective to reduce the torque ripple.

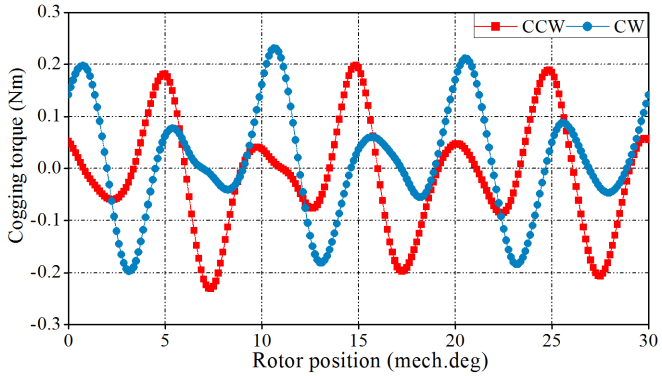

Fig. 8. Cogging torque comparison for two rotation directions.

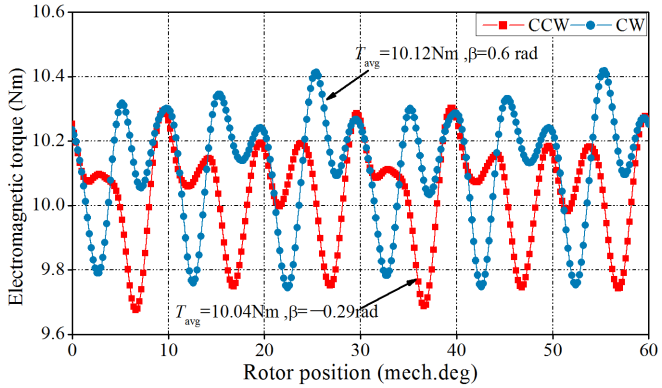

Fig. 9. Electromagnetic torque from different rotatory directions.

IV. Evaluation of Clockwise Torque Characteristics

Fig. 8 compares the cogging torque from different rotatory directions. It is worth noticing that the peak-to-peak value of cogging torque remains practically the same. There exists the significant phase shifting between the two waveforms.

Fig. 9 compares the electromagnetic torque from different rotatory directions. When the machine rotates CW, the torque ripple is 6.67%, 0.41% higher than that when it rotates CCW. The average torque remains practically constant. However, it is worth noticing that the current phase angle β has shifted significantly due to phase shifting of air-gap flux density waveform.

V. Experimental Results

A motor prototype has been manufactured for test. A mass-production PM machine stator is selected, which was designed in the previous project. Rotor laminations were cut by the wire cutting machine; and the laminations are stacked up for rotor core. Fig. 10 shows the photographs of the rotor lamination, the assembled rotor, and the experimental setup. A high-performance torque sensor (Kistler) is adopted in this paper. The cogging torque is measured in no load, and dc motor with reducing mechanism runs at 1 r/min. Fig. 11 shows the measured cogging torque waveform. The peak-to-peak value of cogging torque is 0.48 N · m, which is slightly higher than the FE predicted one. The measured waveform shows the similar variation trend with

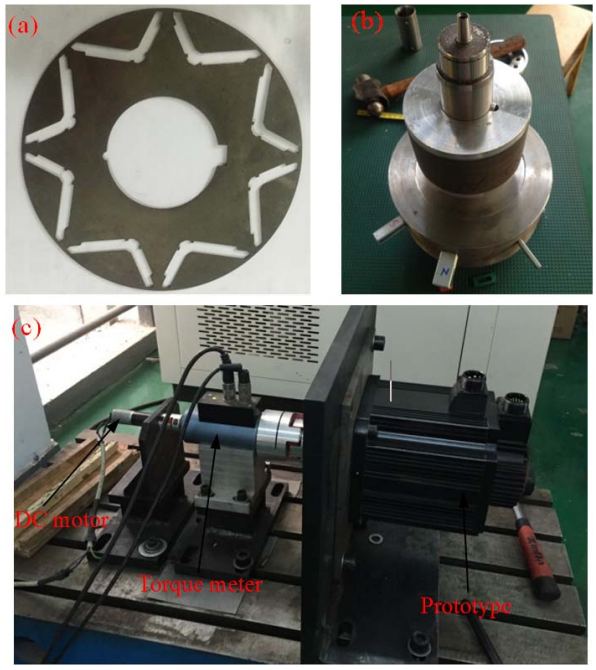

Fig. 10. (a) Rotor lamination. (b) Assembled rotor. (c) Experimental setup.

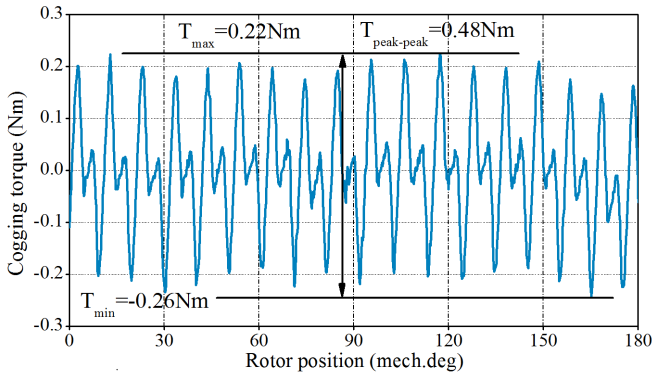

Fig. 11. Measured cogging torque waveform.

the predicted one. FEA model is built based on ideal machine without any manufacture and assembly errors, which are inevitable in actual manufacturing process. In addition, the errors were also not neglected due to experimental setup and instrument. Taking all factors in account, good agreement of the predicted and measured results is obtained. It validates the effectiveness of the proposed rotor in this paper.

VI. Conclusion

A novel asymmetrical V-type rotor configuration is adopted in this paper to reduce the cogging torque and the torque ripple of IPM machine. This rotor structure exhibits satisfactory torque characteristics, without the limitation to rotation direction. The hybrid design of experiment is utilized for rotor optimization, and the final rotor geometry is determined. The proposed rotor gives the main contributor to the reduction of cogging torque and torque ripple. A prototype has been manufactured for test. The appreciable agreement between predicted and measured results has been obtained, which confirms the effectiveness of proposed rotor.

REFERENCES

[1] C. Bianchini, F. Immovilli, E. Lorenzani, A. Bellini, and M. Davoli, "Review of design solutions for internal permanent-magnet machines cogging torque reduction," *IEEE Trans. Magn.*, vol. 48, no. 10, pp. 2685–2693, Oct. 2012.

[2] L. Hao, M. Lin, D. Xu, N. Li, and W. Zhang, "Cogging torque reduction of axial-field flux-switching permanent magnet machine by rotor tooth notching," *IEEE Trans. Magn.*, vol. 51, no. 11, Nov. 2015, Art. no. 8208304.

[3] W. Zhao, T. A. Lipo, and B.-I. Kwon, "Torque pulsation minimization in spoke-type interior permanent magnet motors with skewing and sinusoidal permanent magnet configurations," *IEEE Trans. Magn.*, vol. 51, no. 11, Nov. 2015, Art. no. 8110804.

[4] Z. Q. Zhu, S. Ruangsinchaiwanich, N. Schofield, and D. Howe, "Reduction of cogging torque in interior-magnet brushless machines," *IEEE Trans. Magn.*, vol. 39, no. 5, pp. 3238–3240, Sep. 2003.

[5] S.-K. Lee, G.-H. Kang, J. Hur, and B.-W. Kim, "Stator and rotor shape designs of interior permanent magnet type brushless DC motor for reducing torque fluctuation," *IEEE Trans. Magn.*, vol. 48, no. 11, pp. 4662–4665, Nov. 2012.

[6] G.-H. Kang, Y.-D. Son, G.-T. Kim, and J. Hur, "A novel cogging torque reduction method for interior-type permanent-magnet motor," *IEEE Trans. Ind. Appl.*, vol. 45, no. 1, pp. 161–167, Jan./Feb. 2009.

[7] L. Fang, S.-I. Kim, S.-O. Kwon, and J.-P. Hong, "Novel double-barrier rotor designs in interior-PM motor for reducing torque pulsation," *IEEE Trans. Magn.*, vol. 46, no. 6, pp. 2183–2186, Jun. 2010.

[8] H.-S. Chen, D. G. Dorrell, and M.-C. Tsai, "Design and operation of interior permanent-magnet motors with two axial segments and high rotor saliency," *IEEE Trans. Magn.*, vol. 46, no. 9, pp. 3664–3675, Sep. 2010.

[9] K.-C. Kim, "A novel method for minimization of cogging torque and torque ripple for interior permanent magnet synchronous motor," *IEEE Trans. Magn.*, vol. 50, no. 2, Feb. 2014, Art. no. 7019604.

[10] L. Dosiek and P. Pillay, "Cogging torque reduction in permanent magnet machines," *IEEE Trans. Ind. Appl.*, vol. 43, no. 6, pp. 1565–1571, Nov./Dec. 2007.

[11] W. Ren, Q. Xu, and Q. Li, "Asymmetrical V-shape rotor configuration of an interior permanent magnet machine for improving torque characteristics," *IEEE Trans. Magn.*, vol. 51, no. 11, Nov. 2015, Art. no. 8113704.